Doc Code: AP.PRE.REQ

PTO/SB/33 (07-05)
Approved for use through xx/xx/200x. OMB 0651-00xx
U.S. Patent and Trademark Office; U.S. DEPARTMENT OF COMMERCE

PRE-APPEAL BRIEF REQUEST FOR REVIEW

Docket Number (Optional): JMYT-347US

I hereby certify that this correspondence is being deposited with the United States Postal Service with sufficient postage as first class mail in an envelope addressed to "Mail Stop AF, Commissioner for Patents, P.O. Box 1450, Alexandria, VA 22313-1450" [37 CFR 1.8(a)]

on April 20, 2007

Signature: Lisa Bennett

Typed or printed name: Lisa Bennett

Application Number	Filed
10/527,634	October 7, 2005

First Named Inventor: Martyn Vincent Twigg

Art Unit	Examiner
3748	Tu Minh Nguyen

Applicant requests review of the final rejection in the above-identified application. No amendments are being filed with this request.

This request is being filed with a notice of appeal.

The review is requested for the reason(s) stated on the attached sheet(s).
Note: No more than five (5) pages may be provided.

I am the

- [ ] applicant/inventor.
- [ ] assignee of record of the entire interest. See 37 CFR 3.71. Statement under 37 CFR 3.73(b) is enclosed. (Form PTO/SB/96)
- [x] attorney or agent of record. Registration number 36,201.
- [ ] attorney or agent acting under 37 CFR 1.34. Registration number if acting under 37 CFR 1.34 _____

Signature

Christopher R. Lewis
Typed or printed name

(610) 407-0700
Telephone number

April 20, 2007
Date

NOTE: Signatures of all the inventors or assignees of record of the entire interest or their representative(s) are required. Submit multiple forms if more than one signature is required, see below*.

- [ ] *Total of _____ forms are submitted.

IN THE UNITED STATES PATENT AND TRADEMARK OFFICE

Appln. No:	10/527,634
Applicants:	Martyn Vincent Twigg et al.
Filed:	October 7, 2005
Title:	COMPRESSION IGNITION ENGINE AND EXHAUST SYSTEM THEREFOR
TC/A.U.:	3748
Examiner:	Tu Minh Nguyen
Confirmation No.:	2199
Docket No.:	JMYT-347US

REASONS FOR PRE-APPEAL BRIEF REQUEST FOR REVIEW

Mail Stop AF
Commissioner for Patents
P.O. Box 1450
Alexandria, VA 22313-1450

Sir:

The Pre-Appeal Brief Request for Review is being filed in response to the Final Office Action mailed on December 29, 2006, and more specifically to address the comments in the Advisory Action of March 13, 2007, explaining the Office Action's basis for rejecting the claims.

Claims 1-3, 13-21, 25, 30-34, and 36-40 are pending in the application.

Issue

The cited reference fails to teach one or more of the features of the Applicants' claimed invention. Thus, the cited reference fails to anticipate the Applicants' claimed invention. More specifically, the cited reference fails to teach the claimed feature of "a catalysed component comprising a flow through substrate monolith" (emphasis added). Nevertheless, the Office, as stated in the Advisory Action, asserts that the wall-flow filter disclosed in the cited reference anticipates Applicants' claimed flow through monolith substrate. Applicants contend that the rejection misconstrues the term "flow through" catalyst substrate by giving this term of art a definition contrary to its well-accepted meaning, in order to form the basis of the rejection.

The Final Rejection

Claims 1, 3, 13, 14, 16-21, 25, 34, and 36-40 stand rejected under 35 U.S.C. § 102(a) as anticipated by PCT Publication No. WO 02/26379 (the English equivalent of which is U.S.

Publication No. 2004/0065078) (collectively "Schafer-Sindlinger"). Claims 2, 15, 32, 30, 31, and 33 stand rejected under 35 U.S.C. § 103(a) as unpatentable over Schafer-Sindlinger in view of legal precedent. Claims 1 and 36 are the independent claims.

The Cited Prior Art

Schafer-Sindlinger discloses "a process for removing carbon dioxide, hydrocarbons and soot particles from lean exhaust gases from an internal combustion engine by using a catalytically coated particle filter." (para. 0001). As disclosed, the particle filter used in Schafer-Sindlinger's invention is a wall flow particle filter. (para. 0027). As the Advisory Action comments set forth, Schafer-Sindlinger, at Figure 1 and as discussed at paragraph 0048, discloses

> [A]n exhaust gas system comprising inlet channels (6), outlet channels (7), and porous channel walls (4), wherein a catalytic coating (8) is applied to a surface of the channel wall of inlet channels. Because each of the inlet channel [*sic*] is blocked at the downstream end, an exhaust gas stream from the inlet channel has to flow through the catalytic coating and the porous channel wall in order to get to the outlet channel, as depicted in Figure 1.

Thus, contrary to the incorrect conclusion in the Advisory Action, the exhaust gas system of Schafer-Sindlinger discloses a wall flow filter as the substrate for filtering out soot particles from the lean exhaust gases from an internal combustion engine.

Remarks/Arguments

Based on the above teaching, the Advisory Action asserts that Schafer-Sindlinger "clearly disclose an exhaust system comprising a catalysed component comprising a *flow through* substrate monolith (4,8)" (emphasis added). Applicants respectfully disagree with the Advisory Action's conclusion that Schafer-Sindlinger discloses a flow through substrate. What is being disclosed in Schafer-Sindlinger is clearly a wall flow substrate. Therefore, Schafer-Sindlinger does not anticipate the pending claims, which are limited to a flow through substrate monolith. Applicants contend that for the Advisory Action to conclude that a wall flow filter reads on a flow through monolith substrate is untenable, as it runs contrary to the well-known, well-accepted definitions for these terms of art.

Applicants contend that the term "flow through" substrate monolith is a term of art that describes a substrate monolith with many small, parallel channels running axially through the

substrate from one end to the other. Applicants submit that this is evidenced in the enclosed paper, entitled "Cellular Monolith Substrates" from the DieselNet Technology Guide pp. 1-7 (1998) (copy enclosed). Specifically, at page 1, second paragraph, the paper states that substrates with parallel channels running axially through the whole substrate are known as "flow through" substrates.

A wall flow filter, on the other hand, operates as disclosed in Schafer-Sindlinger, and as further described in the Advisory Action. Specifically, Schafer-Sindlinger sets forth:

> Differently from normal exhaust gas catalysts, the channels of wall flow filters are alternately blocked at the end faces so that the exhaust gas is forced to flow through the porous channel walls on its route from the inlet end face to the outlet end face. The soot particles are filtered out of the exhaust gas stream in this way. Thus, wall flow filters have two sets of flow channels--inflow channels which are open at the inlet end face and blocked at the outlet end face and outflow channels which are blocked at the inlet end face and open at the outlet end face. (Schafer-Sindlinger, para 27).

To illustrate the two different devices, Applicants provide the following Figure, from T.W. Wu et al., "Boundary Element Analysis of Reactive Mufflers and Packed Silencers with Catalyst Converters," page 222 (copy of article enclosed) which shows a through-flow (or flow through) substrate (A) and a wall-flow filter (B):

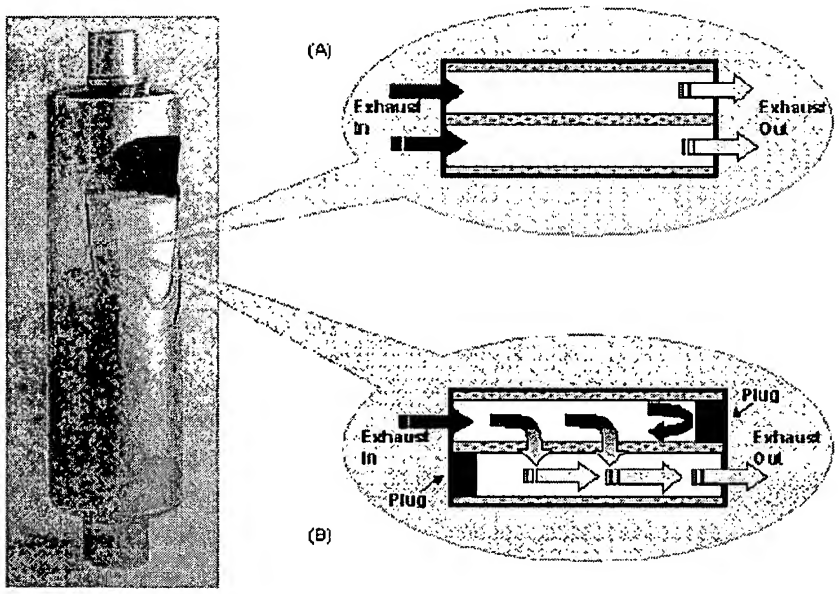

Figure 2 Emission control device with (A) a through-flow catalyst converter (CC), (B) a wall-flow diesel particulate filter (DPF).

Clearly, as shown above, as described in Schafer-Sindlinger, and as is well-known in the art (evidenced by the DieselNet Technology Guide publication), a wall flow filter cannot anticipate a flow through monolith substrate. Not only are flow through substrates structurally different from wall flow filters, but the principle of operation of a wall-flow filter is also markedly different from a flow through monolith substrate.

Moreover, merely by stating, as the Advisory Action asserts, that "an exhaust gas stream from the inlet channel wall has to flow through the catalytic coating and the porous channel wall in order to get to the outlet channel," does not make a "wall flow" filter a "flow through" monolith substrate. The interpretation given by the Advisory Action ignores the significance attributed by these terms of art as denoting specific structures and the different principles of operation attributed to these structures. Such an interpretation clearly ignores the well-established, art-accepted meanings denoted by these terms.

Furthermore, Applicants contend that the use of a flow through substrate monolith in the exhaust system of Schafer-Sindlinger would change the principle of operation of Schafer-Sindlinger. For example, the wall flow filters of Schafer-Sindlinger have porous channel walls to allow the exhaust gas to flow across the channel walls as the exhaust gas proceeds from the inlet to the outlet. (*see* para 36). Flow through filters do not require such porous channels as the exhaust gas flows directly from the inlet to the outlet within the same channel. "If the proposed modification or combination of the prior art would change the principle of operation of the prior art invention being modified, then the teachings of the references are not sufficient to render the claims *prima facie* obvious." *See* M.P.E.P. § 2143.01 (*citing In re Ratti*, 270 F.2d 810, 123 U.S.P.Q. 349 (C.C.P.A. 1959)). Here, not only does Schafer-Sindlinger fail to disclose a flow through substrate monolith, but it would also be improper for the Office to merely assert that Schafer-Sindlinger could substitute a flow through substrate monolith for its wall flow filter. Therefore, Applicants contend that Schafer-Sindlinger does not anticipate, nor could Schafer-Sindlinger render obvious, Applicants' invention as claimed in independent claims 1 and 36.

Dependent claims 2, 3, 13-21, 25, 30-34, and 37-40 are also patentable over the cited references at least for the same reasons that independent claims 1 and 36, on which they are dependent, are patentable, but may be separately patentable for additional reasons as well.

Regarding the obviousness rejections of the dependent claims, based on Schafer-Sindlinger in view of legal precedent, citing to *In re Aller*, because the legal precedent fails to

teach the shortcomings of Schafer-Sindlinger, including disclosing at least a flow through substrate monolith, the Applicants submit that these claims are neither taught nor suggested by Shafer in view of legal precedent. The Office is respectfully asked to withdraw the obviousness rejection as well.

Conclusion

In view of the arguments set forth above, Applicants respectfully submit that the currently pending claims are allowable. Withdrawal of the final rejection is hereby respectfully requested.

Respectfully submitted,

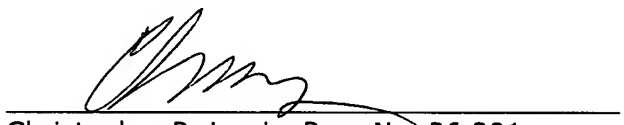

Christopher R. Lewis, Reg. No. 36,201
James C. Abruzzo, Reg. No. 55,890
Attorneys for Applicants

JCA/lrb
Enclosures: Copy of "Cellular Monolith Substrates," DieselNet Technology Guide, pp. 1-7 (1998).
Copy of "Boundary Element Analysis of Reactive Mufflers and Packed Silencers with Catalyst Converters," Electronic Journal of Boundary Elements, Vol. 1, No. 2, pp. 218-235 (2003).

Dated: April 20, 2007

P.O. Box 980
Valley Forge, PA 19482-0980
(610) 407-0700

The Director is hereby authorized to charge or credit Deposit Account No. **18-0350** for any additional fees, or any underpayment or credit for overpayment in connection herewith.

I hereby certify that this correspondence is being deposited with the United States Postal Service as first class mail, with sufficient postage, in an envelope addressed to: Commissioner for Patents, P.O. Box 1450, Alexandria, VA 22313-1450 on:

April 20, 2007
Date

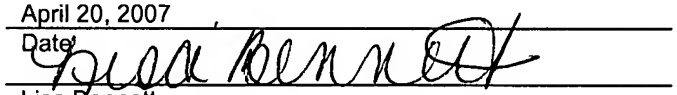

Lisa Bennett

LRB_DOCUMENT2

T. W. Wu / Electronic Journal of Boundary Elements, Vol. I, No. 2, pp. 218-235 (2003)

Boundary Element Analysis of Reactive Mufflers and Packed Silencers with Catalyst Converters

T. W. Wu
Department of Mechanical Engineering, University of Kentucky, Lexington, KY 40506, U.S.A.
E-mail: timwu@engr.uky.edu

C. Y. R. Cheng
Nelson Industries, Inc., Stoughton, WI 53589, U.S.A.

Abstract

This paper reviews recent developments in the application of the boundary element method (BEM) to muffler and silencer analysis. Initial results of modeling built-in catalyst converters are also presented. A so-called "direct mixed-body boundary element method" has been developed for muffler and silencer analysis since 1996. The idea of the method is to integrate all kinds of different boundary and internal surfaces into a single integral equation set without using the conventional multi-domain approach, even though there may be different media in the domain. A key ingredient in this method is the hypersingular integral equation. The concept of the direct mixed-body BEM is not totally against the conventional multi-domain BEM, though. For very large structures or at high frequencies, a multi-domain or substructuring approach is still necessary in order to reduce the memory usage as well as the computation time. With the direct mixed-body BEM, each substructure does not need to be a well-defined and homogeneous subdomain. As such, substructuring can be done more naturally along the longitudinal direction. Catalyst converters may also be modeled as a modular in the general framework of substructuring. Several test cases are presented with experimental verification, including two cases with built-in converters.

Introduction

Reactive mufflers and packed silencers used in industry usually contain very complex internal components such as extended inlet/outlet tubes, thin baffles, perforated tubes, and bulk-reacting sound absorbing materials. Although the interior fluid domain is bounded, the boundary element method (BEM) is still an ideal analysis tool due to its surface-only meshing scheme. Since 1996, Wu and his co-workers [1,2] have used a so-called "direct mixed-body BEM" for the analysis of reactive mufflers with thin internal components and perforated tubes. A key ingredient in the direct mixed-body BEM is the hypersingular integral equation. The use of the hypersingular integral equation for thin-body scattering problems has been a well-known technique. Back in 1980, Terai [3] presented a regularization technique for 3-D planar (and constant)

elements to model acoustic scattering from thin plates. Later, Rizzo and his co-workers were among the pioneers to develop general regularization techniques for curvilinear (and higher-order) boundary elements [4-10]. The general regularization procedure for curvilinear elements has enabled more accurate boundary modeling for complex geometry. The regularization technique was adopted in the direct mixed-body BEM to model thin components and perforated tubes inside reactive mufflers [1,2]. It is noted that the modeling of perforated tubes is similar to the modeling of thin bodies except that an empirical transfer impedance is introduced to relate the pressure jump to the normal velocity [11].

For packed silencers, the BEM modeling becomes even more challenging because there are at least two different acoustic media involved, air and the bulk-reacting sound absorbing material. A bulk-reacting sound absorbing material is characterized by a complex speed of sound and a complex mean density [12]. These two material properties are related to the propagation constant and the characteristic impedance which can be measured by the two-cavity method [12] or approximated by empirical formulas if the flow resistivity of the material is known [13]. The traditional modeling approach is to use the multi-domain BEM [14] in which each subdomain contains only one material. However, the internal geometry of a typical packed silencer is usually quite complex and there may be too many subdomains intricately connected together. It is impractical to define so many subdomains and try to match the boundary conditions at all interfaces. To overcome the modeling difficulty, Wu and his co-workers [15,16] have recently extended the direct mixed-body BEM to packed silencers. The idea is similar to the technique used for reactive mufflers. Boundary integral equations for different subdomains (including those with different material properties) are summed up first. Hypersingular integral equations are then added at interfaces to make up for any missing equations. Because the integral equations for all subdomains are summed up, a multi-domain problem can now be solved in a single-domain fashion. There is no need to define different subdomains or artificial interfaces anymore.

Figure 1 shows a typical packed silencer configuration that can be solved by the direct mixed-body BEM. With reference to the figure, Ω denotes the interior acoustic domain of the silencer. The symbols R, T, P, B, I, IP, IPC, ATB, and BTB represent "Regular", "Thin", "Perforated", "Bulk-reacting", "Interface", "Interface with Perforated surface", "Interface with Perforated surface and Cloth", "Air-Thin-Bulk-reacting", and "Bulk-reacting-Thin-Bulk-reacting" surfaces, respectively. The R surfaces include the exterior silencer surfaces (with no bulk-reacting packing), the external inlet/outlet tubes, and the inlet/outlet ends. The T surfaces are the thin components inside the silencer, such as the extended inlet/outlet tubes, thin baffles, thin flow plugs, and internal connecting tubes. Note that a T surface has air on both sides of the thin surface. The P surfaces are designated for perforated tubes or any perforated thin plates with air on both sides. The B surfaces are the exterior boundary surfaces of the bulk-reacting lining. The I surfaces are the interfaces between the bulk-reacting material and air. The IP surfaces are the perforated interfaces between the bulk-reacting material and air. The IPC interfaces are the same as the IP interfaces except

that a layer of protective cloth is inserted between the perforated plate and the bulk-reacting material to protect the bulk-reacting material from being blown out [16]. The ATB surfaces represent any rigid thin plates between the bulk-reacting material and air. The BTB surfaces represent any embedded rigid thin plates with the bulk-reacting material on both sides.

One unique feature of all direct boundary integral formulations is that it is permissible to use discontinuous elements. With discontinuous elements, a BEM model can be easily assembled from components without worrying about junction continuity, and the mesh can be automatically refined at each frequency. Curvilinear constant elements have been used in the direct mixed-body BEM for muffler and silencer analysis. A coarse mesh is usually used for low-frequency analysis, and the mesh is gradually refined by a simple algorithm as the frequency goes up. This can save a tremendous amount of CPU time as well as mesh preparation time. It should be noted that the surface type naming (such as R, T, P, B, etc in Figure 1) in the direct mixed-body BEM is easy to do and does not require extra preprocessing efforts. When a piece of component mesh is being assembled to the model, its surface type can be attached at the same time. As the mesh is automatically refined later at higher frequencies, the surface type will be carried over.

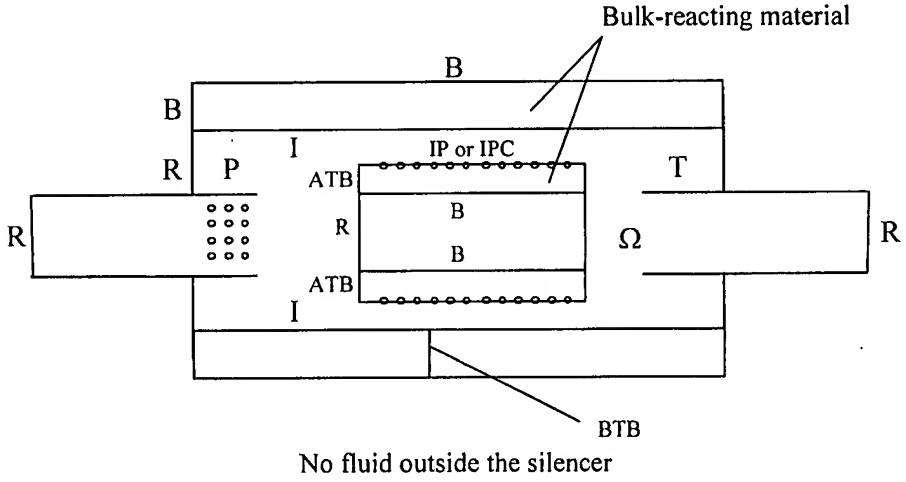

Figure 1 Types of surfaces modeled in the direct mixed-body BEM

It should be noted that when the direct mixed-body BEM for muffler analysis was first presented in 1996 [1], it was meant to eliminate the tedious multi-domain BEM zoning and interface matching so that a muffler model with complicated internal components could be created and solved quickly in a single computation. However, as frequency and the number of elements increase, a large silencer model cannot be computed on a PC or workstation anymore mainly due to the physical limitation of available computer memory, and also partially due to the incredibly long CPU time it will take to finish the

computation. Therefore, dividing a large silencer into smaller substructures so that each substructure can fit into the computer memory one at a time becomes necessary. The BEM first computes the impedance matrix of each substructure one by one. Then, the impedance matrices for substructures are combined by a synthesis procedure to form the resultant impedance matrix for the whole structure [17]. It is noted that in reality the substructuring procedure is nothing but the multi-domain BEM implemented in a modular way. This may sound like some kind of reincarnation of the old multi-domain BEM which we have tried very hard to get rid of and replace with the direct mixed-body BEM. Fortunately, the concept of the direct mixed-body BEM is not totally against the multi-domain BEM, though. In a very recent implementation [18], it is shown that the direct mixed-body BEM actually facilitates the substructuring operations. With the direct mixed-body BEM, each substructure may contain very complex internal components (such as thin and perforated components) as well as bulk-reacting materials. As a result, substructuring can be done more naturally in the silencer's longitudinal direction. The traditional multi-domain BEM rule of having to construct homogeneous (single-medium) and well defined (no thin or perforated surfaces) subdomains are no longer required. That means substructuring can be done more naturally and elegantly with the help of the direct mixed-body BEM.

The substructuring technique introduced in Ref. [18] may also be applied to mufflers and silencers with an inserted acoustic filter element such as a catalytic converter (CC) or a diesel particulate filters (DPF) [19]. A CC or PDF consists of a stack of capillary tubes inserted between two connecting ducts (substructures). Monoliths used in a CC are categorized as through-flow monoliths in which the substrate is made up by a large number of small parallel tubes (or cells) allowing exhaust gas to flow from one end to the other. The substrate is coated with a layer of wash coat material and catalyst to enhance the catalytic function. As the exhaust gas flows through the catalyst, gaseous pollutants such as nitrous oxide (NOx), carbon monoxide (CO), hydrocarbons (HC) are converted into less harmful gases. Monoliths used in DPF are known as wall-flow monoliths in which exhaust gas is forced to flow through porous tube walls. The removal of soot particles is accomplished by the filtration process in which the wall pores filter out the particulate. Figure 2 shows the comparison between a CC and a DPF.

To model a CC, a four-pole transfer matrix can be used to represent the connection between the two connecting substructures (one before the CC and one after). As will be shown in this paper, the transfer matrix is a diagonal matrix with an appropriate set of four-pole parameters derived from the one-dimensional plane-wave theory. The characteristic impedance and the propagation constant of the converter can be measured by the two-cavity method. The diagonal matrix actually represents an "element-to-element" connection between the two connecting substructures separated by the CC. Compared to the CC, the DPF is harder to model due to its wall-flow nature. Rigorously speaking, the one-dimensional plane-wave theory is actually not valid inside the DPF because of the alternate plugs at the inlet and outlet ends. Nevertheless, if we assume that sound waves will penetrate only the neighboring capillary tubes and quickly get out from there due to the least resistance, then the 1-D

"element-to-element" four-pole connection may still be a good approximation for the DPF.

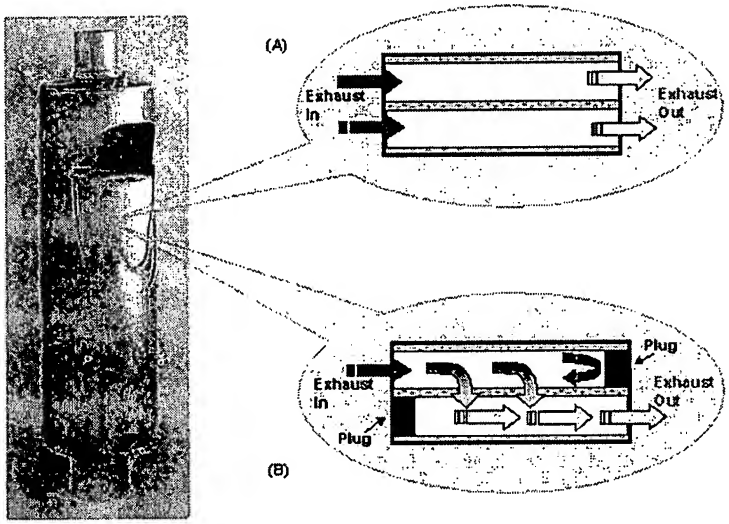

Figure 2 Emission control device with (A) a through-flow catalyst converter (CC), (B) a wall-flow diesel particulate filter (DPF).

In this paper, we first present the boundary integral equations for the direct mixed-body BEM followed by the impedance matrix synthesis used in the substructuring BEM. The connection between two neighboring substructures can be either a four-pole transfer matrix (for a CC or DPF) or simply an identity matrix (for direct connection). Several test cases including two with an inserted CC/DPF are presented to demonstrate the substructuring technique. Numerical results are compared to experimental measurements.

Direct Mixed-Body BEM

The governing differential equations for a two-medium acoustic problem as depicted in Figure 1 are

$$\nabla^2 p + k_A^2 p = 0 \qquad \text{in air} \tag{1}$$

$$\nabla^2 p + k_B^2 p = 0 \qquad \text{in the bulk-reacting material} \tag{2}$$

where p is the sound pressure, and k_A and k_B are the wavenumbers in air and the bulk-reacting material, respectively. The corresponding fundamental solutions are

$$\psi_A = \frac{e^{-ik_A r}}{r} \tag{3}$$

$$\psi_B = \frac{e^{-ik_B r}}{r} \tag{4}$$

where $i = \sqrt{-1}$ and r is the distance between the collocation point P and any surface point Q.

Let ω be the angular frequency, ρ_A, ρ_B, c_A, and c_B be the mean density and speed of sound of air and the bulk-reacting material, respectively. Let n be the unit normal vector. The normal vector on the R or B boundary is pointing into the interior acoustic domain, and on the I, IP, IPC, and ATB interfaces the normal vector is pointing into the air side. On T, P, and BTB, the normal vector can be pointing into either side; the side into which the normal is pointing is called the positive side, and the corresponding pressure is denoted by p^+. The other side of T, P. or BTB is called the negative side and the pressure there is denoted by p^-. Without going through the derivation details, the complete boundary integral equations are given in the following [15,16,18]:

$$\begin{aligned}
&\int_R (p\frac{\partial \psi_A}{\partial n} + i\rho_A \omega v_n \psi_A) dS + \int_{T+P} \frac{\partial \psi_A}{\partial n}(p^+ - p^-) dS \\
&+ \int_B (p\frac{\partial \psi_B}{\partial n} + i\rho_B \omega v_n \psi_B) dS + \int_{BTB} \frac{\partial \psi_B}{\partial n}(p^+ - p^-) dS \\
&+ \int [p(\frac{\partial \psi_A}{\partial n} - \frac{\partial \psi_B}{\partial n}) + i\omega v_n(\rho_A \psi_A - \rho_B \psi_B)] dS \\
&+ \int_{P+IPC} [p_A(\frac{\partial \psi_A}{\partial n} - \frac{\partial \psi_B}{\partial n}) - \rho_A c_A \xi^* v_n \frac{\partial \psi_B}{\partial n} + i\omega v_n(\rho_A \psi_A - \rho_B \psi_B)] dS \\
&+ \int_{ATB} (p_A \frac{\partial \psi_A}{\partial n} - p_B \frac{\partial \psi_B}{\partial n}) dS
\end{aligned}$$

$$= \begin{cases}
4\pi p(P) & P \in \Omega & (5a) \\
2\pi p(P) & P \in \mathrm{R} + \mathrm{B} & (5b) \\
2\pi[p^+(P) + p^-(P)] & P \in \mathrm{T} + \mathrm{P} + \mathrm{BTB} & (5c) \\
4\pi p(P) & P \in \mathrm{I} & (5d) \\
4\pi p_A(P) + 2\pi \rho_A c_A \xi^* v_n(P) & P \in \mathrm{IP} + \mathrm{IPC} & (5e) \\
2\pi[p_A(P) + p_B(P)] & P \in \mathrm{ATB} & (5f)
\end{cases}$$

and

$$\int_R (p\frac{\partial^2\psi_A}{\partial n\partial n^P} + i\rho_A\omega v_n\frac{\partial\psi_A}{\partial n^P})dS + \int_{T+P}\frac{\partial^2\psi_A}{\partial n\partial n^P}(p^+ - p^-)dS$$
$$+ \int_B (p\frac{\partial^2\psi_B}{\partial n\partial n^P} + i\rho_B\omega v_n\frac{\partial\psi_B}{\partial n^P})dS + \int_{BTB}\frac{\partial^2\psi_B}{\partial n\partial n^P}(p^+ - p^-)dS$$
$$+ \int [p(\frac{\partial^2\psi_A}{\partial n\partial n^P} - \frac{\partial^2\psi_B}{\partial n\partial n^P}) + i\omega v_n(\rho_A\frac{\partial\psi_A}{\partial n^P} - \rho_B\frac{\partial\psi_B}{\partial n^P})]dS$$
$$+ \int_{P+IPC}[p_A(\frac{\partial^2\psi_A}{\partial n\partial n^P} - \frac{\partial^2\psi_B}{\partial n\partial n^P}) - \rho_A c_A\xi^* v_n\frac{\partial^2\psi_B}{\partial n\partial n^P} + i\omega v_n(\rho_A\frac{\partial\psi_A}{\partial n^P} - \rho_B\frac{\partial\psi_B}{\partial n^P})]dS$$
$$+ \int_{ATB}(p_A\frac{\partial^2\psi_A}{\partial n\partial n^P} - p_B\frac{\partial^2\psi_B}{\partial n\partial n^P})dS$$

$$= \begin{cases} 0 & P \in \mathrm{T+BTB+ATB} \quad (6a) \\ 4\pi\frac{ik_A}{\xi}[p^+(P) - p^-(P)] & P \in \mathrm{P} \quad (6b) \\ -2\pi i\omega(\rho_A + \rho_B)v_n(P) & P \in \mathrm{I+IP+IPC} \quad (6c) \end{cases}$$

where ξ is the dimensionless transfer impedance for perforated tubes or perforated surfaces [11], and ξ^* is the dimensionless transfer impedance for IP or IPC interfaces. On an IP interface, ξ^* is identical to ξ. On an IPC interface, ξ^* is the sum of ξ and the dimensionless transfer impedance of the protective cloth [16].

Substructuring Using the Impedance Matrix Synthesis (IMS)

To begin with, we assume that a silencer is divided into two substructures as shown in Fig. 3. It is possible that the two substructures are connected to each other by a built-in acoustic filter element represented by the dotted lines in Fig. 3. Let p_i and v_i denote the sound pressure and the particle velocity in the longitudinal direction, respectively, at the inlet of the first substructure, and p_o and v_o denote the corresponding variables at the outlet of the second substructure. Also, p_1 and v_1 are the variables at the outlet of the first substructure, and p_2 and v_2 are at the inlet of the second substructure. It should be noted that sound pressure and particle velocity may not be uniform at any cross section. Therefore, each p and v variable used in this section actually represents a vector. The length of each vector depends on the number of elements used at each cross section.

For substructure 1, the sound pressures at the inlet and the outlet are related to the corresponding particle velocities by an impedance matrix

$$\begin{bmatrix} p_i \\ p_1 \end{bmatrix} = \begin{bmatrix} Z_{11} & Z_{12} \\ Z_{21} & Z_{22} \end{bmatrix} \begin{bmatrix} v_i \\ v_1 \end{bmatrix} \tag{7a}$$

$$\tag{7b}$$

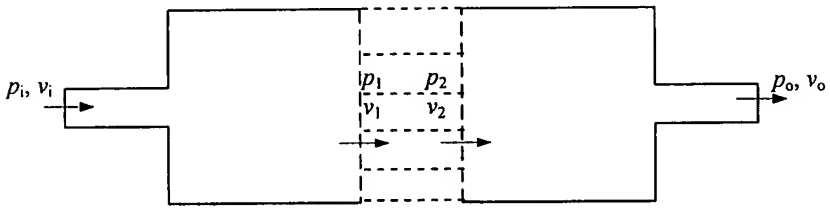

Figure 3 Two substructures connected by an acoustic filter element.

It is important to note that the linear relationship of the above equation is true only when the rest of the boundary of substructure 1 is either rigid or just has an impedance boundary condition. To obtain the impedance matrix, one will need to run the BEM on substructure 1 with a multiple of velocity boundary conditions. For example, to obtain the first column of the impedance matrix, v=1 is applied to the first element at the inlet of substructure 1, and v=0 is applied elsewhere. The sound pressure solutions at the inlet and outlet will become the first column of the impedance matrix. Similarly, by making v=1 on each element at the inlet and outlet one at a time, the whole impedance can be obtained. It seems that to obtain the complete impedance matrix of Eq. (7) one would have to run the BEM on the substructure for a multiple of times, with a different velocity boundary condition each time. However, it should be noted that only one BEM matrix needs to be formed and decomposed at each frequency. The vectors on the right-hand side of the matrix corresponding to different velocity boundary conditions can be generated at the same time, and each different right-hand side vector only requires a trivial back substitution.

Similarly, one can create the impedance matrix for substructure 2. The impedance matrix relationship is

$$\begin{bmatrix} p_2 \\ p_o \end{bmatrix} = \begin{bmatrix} Z_{31} & Z_{32} \\ Z_{41} & Z_{42} \end{bmatrix} \begin{bmatrix} v_2 \\ v_o \end{bmatrix} \tag{8a}$$

$$\tag{8b}$$

For the acoustic filter element that connects the two substructures, a four-pole transfer matrix is used to describe the acoustic property of the filter element. That is,

$$\begin{bmatrix} p_1 \\ v_1 \end{bmatrix} = \begin{bmatrix} A & B \\ C & D \end{bmatrix} \begin{bmatrix} p_2 \\ v_2 \end{bmatrix} \tag{9a}$$

$$\tag{9b}$$

Note that for a through-flow type catalytic monolith, each capillary tube can be assumed to have a rigid wall. Since the diameter of each capillary tube is small, a plane-wave motion that consists of a forward traveling wave and a backward reflective wave is sufficient to describe the behavior in each capillary tube. Due to the rigid-wall assumption, there is no interaction between any two tubes. Under such circumstances, the transfer matrix coefficients A, B, C, and D are each a diagonal matrix. In other words,

$$A = \begin{bmatrix} A_1 & & \\ & A_1 & \\ & & \ddots \\ & & & A_1 \end{bmatrix}, \; B = \begin{bmatrix} B_1 & & \\ & B_1 & \\ & & \ddots \\ & & & B_1 \end{bmatrix}, C = \begin{bmatrix} C_1 & & \\ & C_1 & \\ & & \ddots \\ & & & C_1 \end{bmatrix}, D = \begin{bmatrix} D_1 & & \\ & D_1 & \\ & & \ddots \\ & & & D_1 \end{bmatrix} \tag{10}$$

where A_1, B_1, C_1, and D_1 are the four-pole parameters of a straight tube. With the diagonal matrices in Eq. (10), Eq. (9) actually represents an "element-to-element" connection between the two substructures. To account for resistance and friction loss, the four-pole parameters are expressed in terms of a complex mean density ρ^* and a complex speed of sound c^*. Both material properties can be measured by the two-cavity method on a sample of CC or DPF with the same length (as in real applications). The four-pole parameters for a straight tube are

$$A_1 = \cos k^* L \tag{11a}$$

$$B_1 = i\rho^* c^* \sin k^* L \tag{11b}$$

$$C_1 = \frac{i}{\rho^* c^*} \sin k^* L \tag{11c}$$

$$D_1 = \cos k^* L \tag{11d}$$

where the complex wavenumber $k^* = \omega / c^*$ and L is the length of the CC or DPF.

It should be noted that when the two substructures are in direct contact (without the acoustic filter element in between), the transfer matrix reduces to the identity matrix. In other words, $A=D=I$ and $B=C=0$, where I is the identity matrix.

The interface variables, p_1, v_1, p_2, and v_2, can be eliminated from Eqs. (7)-(9) so that p_i and v_i are directly related to p_o and v_o. The result is

$$\begin{bmatrix} p_i \\ p_o \end{bmatrix} = \begin{bmatrix} Z_{51} & Z_{52} \\ Z_{61} & Z_{62} \end{bmatrix} \begin{bmatrix} v_i \\ v_o \end{bmatrix}, \tag{12}$$

where

$$Z_{51} = Z_{11} + Z_{12}[C(Z_{31}K^{-1}Z_{21}) + DK^{-1}Z_{21}] \tag{13a}$$

$$Z_{52} = Z_{12}C[Z_{32} - Z_{31}K^{-1}(A - Z_{22}C)Z_{32}] - Z_{12}D[K^{-1}(A - Z_{22}C)Z_{32}] \tag{13b}$$

$$Z_{61} = Z_{41}K^{-1}Z_{21} \tag{13c}$$

$$Z_{62} = Z_{42} - Z_{41}K^{-1}(A - Z_{22}C)Z_{32} \tag{13d}$$

with

$$K = \left[(A - Z_{22}C)Z_{31} + (B - Z_{22}D)\right], \tag{14}$$

Note that sound pressure and particle velocity are usually uniform across any cross section in the inlet tube and in the outlet tube as well. That means each of the vectors p_i, v_i, p_o, and v_o can be lumped into one single variable, and the impedance matrix in Eq. (12) can be further reduced to a 4x4 impedance matrix. With the lumped 4x4 impedance matrix ready, the TL of the silencer can be easily obtained [2].

As mentioned earlier, when the two substructures are in direct contact, A=D=I and B=C=0. Equation (14) reduces to

$$K = Z_{31} - Z_{22} \tag{15}$$

and Eqs. (13a-d) become

$$Z_{51} = Z_{11} + Z_{12}(Z_{31} - Z_{22})^{-1}Z_{21} \tag{16a}$$

$$Z_{52} = -Z_{12}(Z_{31} - Z_{22})^{-1}Z_{32} \tag{16b}$$

$$Z_{61} = Z_{41}(Z_{31} - Z_{22})^{-1}Z_{21} \tag{16c}$$

$$Z_{62} = Z_{42} - Z_{41}(Z_{31} - Z_{22})^{-1}Z_{32} \tag{16d}$$

If a silencer is divided into multiple substructures (more than two) in series connection, the impedance matrix synthesis can be first applied to the first two substructures to produce a resulting impedance matrix. Then the resulting impedance matrix is combined with the impedance matrix of the third substructure by the same synthesis method. The procedure is repeated until the last substructure is reached. It is noticed that many packed silencers in practical use may have an identical cross section in a large portion of the silencer structure. For those kinds of silencers, the impedance matrix of a small section of the identical geometry can be used as a "template", which can be repeatedly used in the synthesis procedure.

Test Cases

The first test case is a parallel-baffle silencer [18] as shown in Fig. 4. Both the inlet and the outlet tubes have a diameter of 5". The two transition ducts that connect the inlet/outlet tubes to the parallel-baffle section have a square cross section of varying dimensions.

Figure 4b shows the cross section of the parallel-baffle section. Two 4"x24"x36" Polyester parallel baffles are used as center splitters in a 24"x24"x36" rectangular duct, and two 2"x24"x36" baffles are attached to the two side walls, respectively, as linings. This creates three 4" air gaps in the center. As shown in Fig. 4c, each Polyester splitter is covered by a perforated metal sheet (designated as IP surface) on its sides and a rigid plate (designated as ATB surface) at both ends. The porosity of the IP interfaces is 23%.

Since the model has two planes of symmetry, only a quarter of the silencer geometry has to be modeled. Even so, the whole model still cannot fit in a PC with 1GB memory at high frequencies without dividing the silencer into smaller substructures. It is noticed the parallel-baffle section has an identical cross section over its length except at the two ATB ends (covering plates). Thus, a template as shown in Fig. 5 can be created and its impedance matrix, once computed for each frequency, can be repeatedly used in the synthesis procedure. Figure 6 shows the comparison of the BEM predictions using four and ten substructures and the experimental TL curve. It is seen that the BEM results compare fairly well with the measured TL curve, although some small discrepancies do exist between models with different number of substructures.

The second test case is a catalytic converter (CC) consisting of a ceramic monolith as shown in Fig. 7 [19]. The catalytic monolith is made up of capillaries with square cross-sections and has a cell density of 400 cells per square inch (CPSI). The monolith used in this study is uncoated. A circular substrate sample is cored out from the catalytic monolith in full length for measuring its characteristic impedance and propagation constant using the two-cavity method. There are two ways to make BEM predictions. One is to directly model the CC as a block of homogeneous and isotropic bulk-reacting material (BRM), and the other is to model the CC by the "element-to-element" four-pole transfer matrix as described in the impedance matrix synthesis (IMS) section of this paper. As shown in Fig. 8, both BEM predictions compare reasonably well with the experimental data. Both numerical approaches produce very similar results. The IMS approach, however, generates numerical results much faster than the direct BRM modeling method. Since it is assumed that the acoustic propagation in the catalytic monolith is predominantly one-dimensional, a simple four-pole transfer matrix would be adequate to represent the catalytic monolith. The predicted TL curve for an empty housing without the catalytic monolith is also plotted in the same graph for comparison. The results reveal that the first two domes of the TL curves are the reactive effect caused by wave reflections due to area changes in the housing. Beyond the first two domes, the noise attenuation is dominated by the dissipative effect inside the capillaries of the monolith. The catalytic monolith increases the overall TL by more than 5 dB except for the first dome.

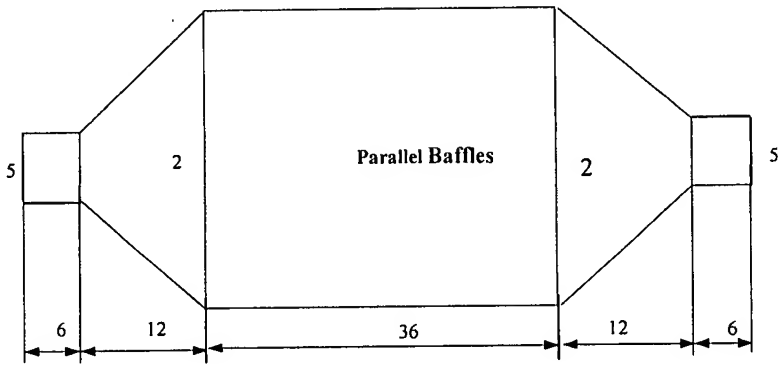

(a) exterior geometry (dimensions in inches)

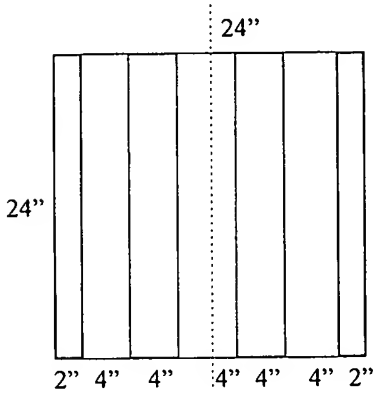

(b) cross section of the parallel baffles

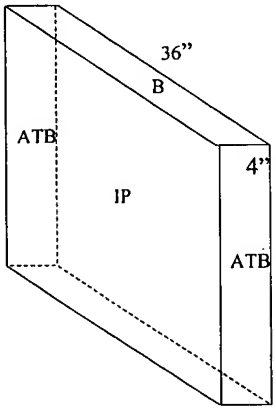

(c) splitter geometry

Figure 4 Parallel-baffle silencer with a lining on both side walls.

Using the same test configuration, the catalytic monolith is replaced by a ceramic wall-flow filter monolith (a DPF) in the third test case [19]. The DPF monolith has a cell density of 100 CPSI and is also uncoated. Figure 9 shows the BEM predictions versus the experimental data. It can be seen that both numerical approaches under-predict the TL values though the trend of the curves agrees well with the experimental results. The discrepancy is due to the fact that sound propagation in the wall-flow monolith is not

limited to only the axial direction along the capillaries. There is significant amount of sound transmission through the walls of the filter monolith.

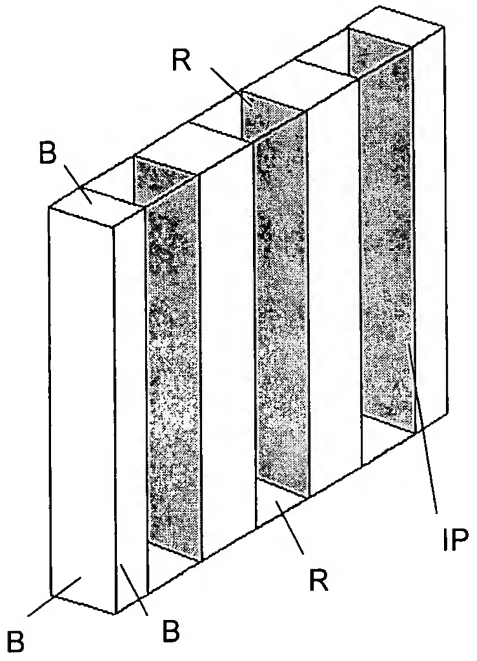

Figure 5 A substructure template created from the identical center portion of the parallel-baffle silencer in Fig. 4.

Conclusions

Recent developments of the direct mixed-body BEM for muffler and silencer analysis are reviewed. A key ingredient in the direct mixed-body BEM is the hypersingular integral equation. It is well known that the hypersingular integral equation is ideally suited to thin-body problems so that a multi-domain approach can be avoided. The direct mixed-body BEM has demonstrated that even a two-medium or multi-medium problem can benefit from the hypersingular integral equation.

Ironically, the direct mixed-body BEM, originally meant to the "terminator" of the old multi-domain BEM, has turned out to be a "facilitator" of the new substructuring technique which is basically a modular implementation of the old multi-domain BEM. For large structures, the combined technique of the direct mixed-body BEM and substructuring has proven to be very effective.

This paper also presents two examples of mufflers with an emission control device such as a CC or DPF. Although the proposed four-pole matrix is very effective for the CC test case, it only provides an approximation for the DPF test case. More research is in order for the modeling of a DPF in the future.

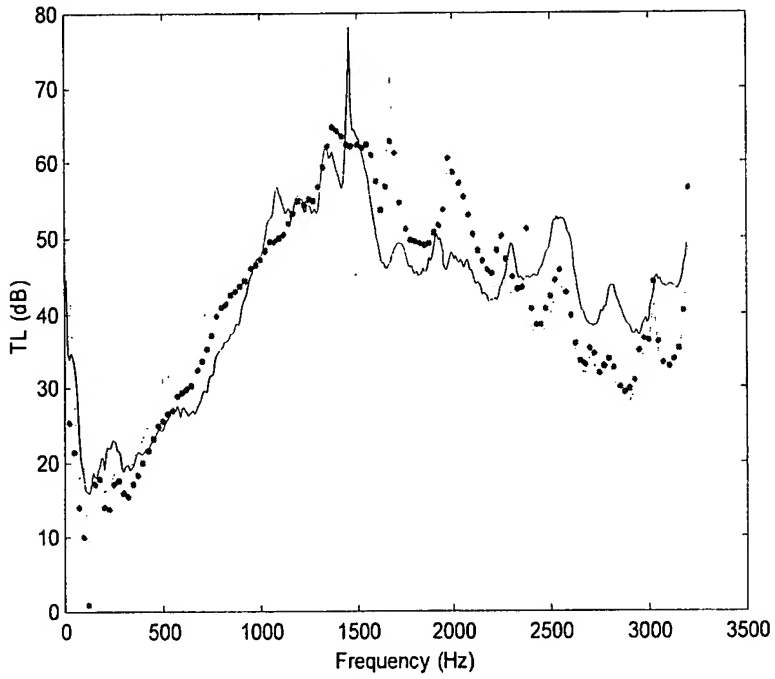

Figure 6 Transmission loss for the parallel-baffle silencer. Solid line: experiment; solid dots: BEM using four substructures; dotted line: BEM using ten substructures.

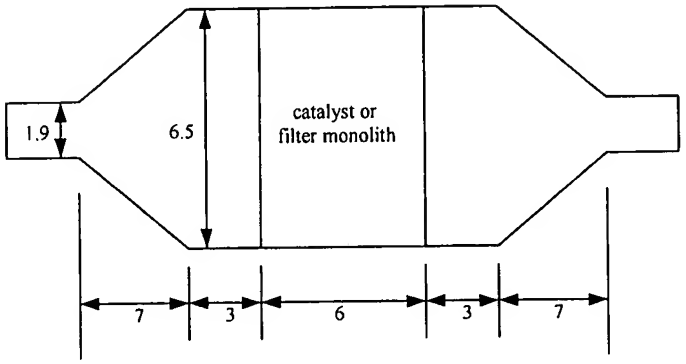

Figure 7 Emission control device test case (dimensions in inches).

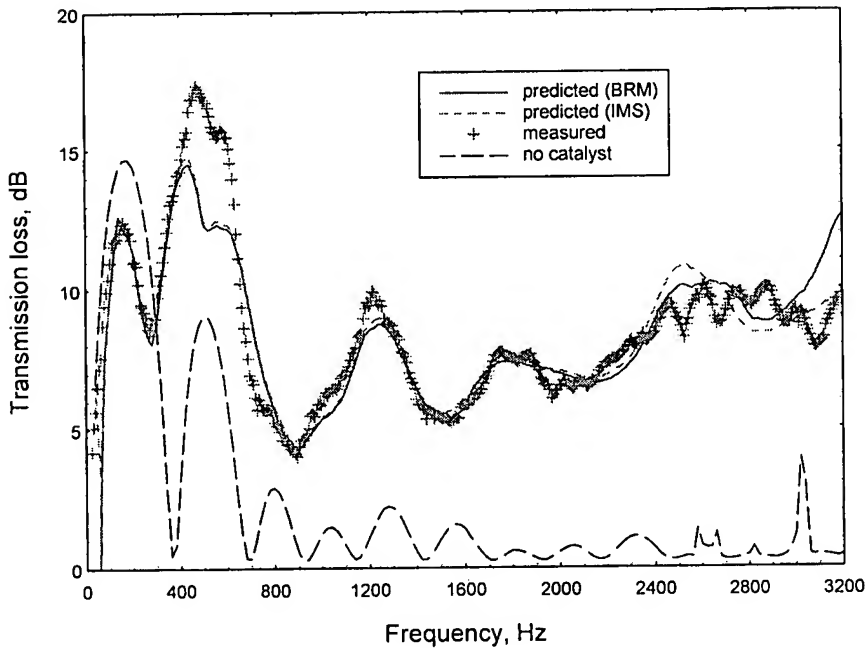

Figure 8 Comparison of the predicted and measured TL of the CC test case.

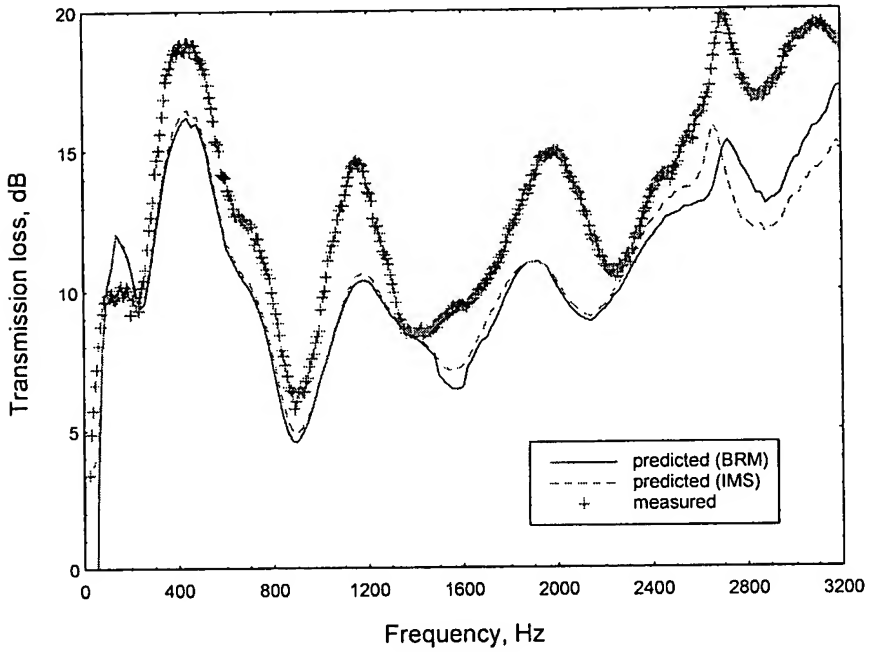

Figure 9 Comparison of the predicted and measured TL of the DPF test case.

Acknowledgement

This research was supported by Nelson Industries (a division of Cummins, Inc.)

References

1. Wu, T. W., Wan, G. C. Muffler performance studies using a direct mixed-body boundary element method and a three-point method for evaluating transmission loss. *Journal of Vibration and Acoustics, ASME Transactions* 1996; 118:479-484.

2. Wu, T. W., Zhang, P., Cheng, C. Y. R. Boundary element analysis of mufflers with an improved method for deriving the four-pole parameters. *Journal of Sound and Vibration* 1998; 217: 767-779.

3. Terai, T. On calculation of sound fields around three dimensional objects by integral equation methods. *Journal of Sound and Vibration* 1980; 69: 71-100.

4. Krishnasamy, G., Schmerr, L. W., Rudolphi, T. J., and Rizzo, F. J. Hypersingular boundary integral equations: some applications in acoustic and elastic wave scattering. *Journal of Applied Mechanics, ASME Transactions* 1990; 57: 404-414.

5. Liu, Y. J. and Rizzo, F. J. A weakly singular form of the hypersingular boundary integral equation applied to 3-D acoustic wave problems. *Computer Methods in Applied Mechanics and Engineering* 1992; 96: 271-287.

6. Guiggiani, M., Krishnasamy, G., Rudolphi, T. J., and Rizzo, F. J. A general algorithm for the numerical solution of hypersingular boundary integral equations. *Journal of Applied Mechanics, ASME Transactions* 1992; 59: 604-614.

7. Liu, Y. J. and Rizzo, F. J. Hypersingular boundary integral equations for radiation and scattering of elastic waves in three dimensions. *Computer Methods in Applied Mechanics and Engineering* 1993; 107: 131-144.

8. Krishnasamy, G., Rizzo, F. J., and Liu, Y. J. Boundary integral equations for thin bodies. *International Journal for Numerical Methods in Engineering* 1994; 37: 107-121.

9. Chao J. C., Liu Y. J., Rizzo F. J., Martin, P. A., and Udpa, L. Regularized integral equations and curvilinear boundary elements for electromagnetic wave scattering in three dimensions. *IEEE Transaction on Antennas and Propagation* 1995; 43:1416-1422.

10. Martin, P. A. and Rizzo, F. J. Hypersingular integrals: How smooth must the density be? *International Journal for Numerical Methods in Engineering* 1996; 39: 687-704.

11. Sullivan, J. W., Crocker, M. J. Analysis of concentric-tube resonators having unpartitioned cavities. *Journal of Acoustical Society of America* 1978; 64:207-215.

12. Utsuno, H., Tanaka, T., Fujikawa, T., Seybert, A. F. Transfer function method for measuring characteristic impedance and propagation constant of porous materials. *Journal of Acoustical Society of America* 1989; 86:637-643.

13. Beranek, L. L., Editor, *Noise and Vibration Control*, Institute of Noise Control Engineering, 1988.

14. Utsuno, H., Wu, T. W., Seybert, A. F., Tanaka, T. Prediction of sound fields in cavities with sound absorbing materials. *AIAA Journal* 1990; 28:1870-1876.

15. Wu, T. W., Cheng, C. Y. R., Zhang, P. A direct mixed-body boundary element method for packed silencers. *Journal of Acoustical Society of America* 2002; 111: 2566-2572.

16. Wu, T. W., Cheng, C. Y. R., Tao Z. Boundary element analysis of packed silencers with protective cloth and embedded thin surfaces. *Journal of Sound and Vibration* 2003; 261:1-15.

17. Ji, Z., Ma, Q., Zhang, Z. Application of the boundary element method to predicting acoustic performance of expansion chamber mufflers with mean flow. *Journal of Sound and Vibration* 1994; 173:57-71.

18. Lou, G., Wu, T. W., and Cheng, C. Y. R. Boundary element analysis of packed silencers with a substructuring technique. *Engineering Analysis with Boundary Elements* 2003; 27: 643-654.

19. Cheng, C. Y. R., Wu, T. W. and Lou, G. Acoustical performance prediction of exhaust emission control devices using BEM. *Inter-Noise 2002*, 2002; Paper N125, on CD.

DieselNet Technology Guide » Emission Control Catalysts

Cellular Monolith Substrates

Abstract: Cellular monoliths replaced the pellet shaped catalyst supports and became the standard substrate for emission control catalysts. The monoliths can be either ceramic extrusions or corrugated metal foil assemblies. Each type is typically coated with an intermediate layer of inorganic oxides, called washcoat, in order to provide the high surface area required for catalysis. Cellular properties of monoliths, such as geometric surface area, open frontal area, and hydraulic diameter are defined in the paper and related to the cell geometry. The influence of substrate geometry on catalyst performance is discussed. The formulas to calculate catalyst substrate pressure drop are given.

1. Catalyst Substrates

Many of the early automotive catalytic converters in the 1970s utilized pellet or bead-shape supports. A volume of spherical particles (pellets) made of gamma-alumina, 2.5 to 5 mm in diameter, was placed into a steel shell and contained between two screens to form the catalytic converter. The noble metal catalyst and stabilizers were incorporated into the pellets. That catalyst design originated from catalytic reactors used in the chemical processing industry. Pelleted catalysts had several disadvantages including high pressure drop and gradual catalyst loss due to attrition. Monolithic honeycombs, which were developed to address the shortcomings of pelleted supports, have become the standard substrate in today's automotive, diesel, and other emission control catalyst applications.

Monolithic catalyst supports are honeycomb structures with many small, parallel channels running axially through the part. They are sometimes called "flow-through" substrates. The cross-section is typically circular or oval, but asymmetric contours are also manufactured. Exhaust gases flowing through the channels contact the catalyst which is deposited on the channel walls. Major advantages of monolithic supports include high geometric surface area (GSA) per unit volume (compactness), large open frontal area (low pressure drop), and excellent attrition resistance.

Monolithic catalyst substrates (Figure 1) are made of ceramics or metal. Ceramic substrates (honeycombs) usually have square cells, while most metallic substrates have sinusoidal channels. Other channel cross sections are possible, including triangular, hexagonal, trapezoidal and round. The number of cells can vary between 10 and over 1000 cells per square inch (cpsi). Parts that were commercially used for internal combustion engine applications in the 1990s had cell densities between 200 and 600 cpsi, with 400 cpsi being the most common cell density in gasoline car applications. Since then, increasingly higher cell densities have been introduced in gasoline cars, with parts in excess of 1000 cpsi being available in both the ceramic [Kikuchi 1999] and metallic designs [Marsh 2001]. Most substrates for diesel applications remain in the 300-400 cpsi range.

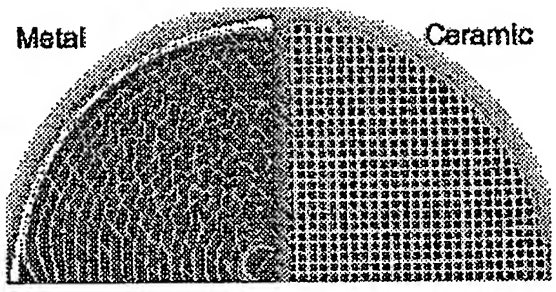

Figure 1. Monolithic Catalyst Substrates

Compared to materials used in catalysis, the walls of ceramic honeycombs have large pores and very low specific surface areas of about 0.3 m^2/g. Foils used for metal substrates have no porosity. Since high surface area carriers are required for catalysts, it is necessary to deposit a high surface area coating onto the channel walls. That coating, called the *washcoat*, is composed of porous, high surface area inorganic oxides such as gamma-Al_2O_3. The specific surface area of the catalyst washcoat materials is typically above 100 m^2/g. Noble metal catalysts, such as platinum, are deposited on the surface and within the pores of the washcoat. Exhaust gases in a catalytic converter diffuse through the washcoat pore structure to the catalytic sites where catalytic reactions occur.

The washcoat layer on a metallic foil and on a ceramic substrate is illustrated in Figure 2. The thickness of the washcoat layer is 20-40 μm. Much thicker washcoat deposits ("fillets") are formed in the cell corners, especially in the sinusoidal channels of metallic substrates. In some technologies, the metal foil is washcoated prior to forming the honeycomb. These technologies produce clean channels with no fillets in the corners but tend to compromise the mechanical strength and durability of the substrate.

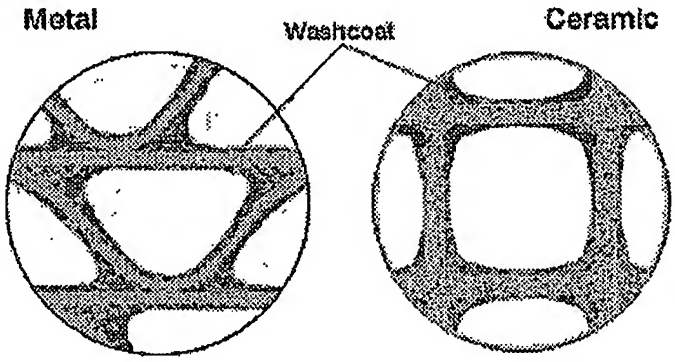

Figure 2. Catalyst Washcoat

Other, non-cellular monolithic substrates have been also researched for catalyst applications. Popular designs include various rigid foams made of cordierite, silicon carbide [Stankiewicz 1998], or metal [Jatkar 1997]. Compared to the honeycomb monoliths, these products have low geometric surface areas and/or high pressure drop. They found very limited commercial use as catalyst substrates.

2. Cellular Properties of Monoliths

A number of terms have been defined to describe the geometrical, mechanical, heat transfer, and hydraulics properties of cellular monoliths. All of these terms are related to the substrate cell geometry.

A square cell matrix, typical for ceramic monoliths, is shown in Figure 3. Most of the cellular monolith properties are derived from, and can be expressed as a function of the cell repeat distance, s, and the wall thickness, w.

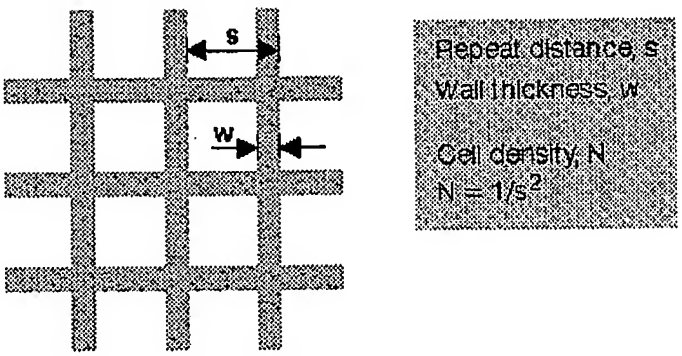

Figure 3. Cell Geometry

Cell density, N, is defined as the number of channels per unit of cross-sectional area. In the case of square cell geometry, it is a simple function of the cell repeated distance, s, as given by Equation (1). Units of cell density are cells per square inch (cpsi) or cells per square centimeter ($1/cm^2$).

$$N = 1/s^2 \qquad (1)$$

Specific geometric surface area (GSA), a_g, is the total channel surface area per unit of substrate volume. It is an important parameter of catalyst substrates which is always specified by the manufacturer. For square cells, it can be calculated from cell geometry using Equation (2).

$$a_g = 4(s - w)/s^2 = 4(1 - w/s)N^{0.5} \qquad (2)$$

Open frontal area (OFA), A_F, is the part of the total substrate cross-section area which is available for the flow of gas. The OFA, which is frequently expressed as a percentage of the total substrate cross-section (and sometimes called the substrate void fraction), is another important parameter always included in the specifications of cellular products. For square cells, the ratio of the open area to the total cross sectional channel area, (A_F/A), is given by Equation (3).

$$A_F/A = (s - w)^2/s^2 = (1 - w/s)^2 \qquad (3)$$

Hydraulic diameter of substrate channels, d_h, is used as a measure of size for non circular channels in all hydraulics, mass transfer and heat transfer calculations. The definition of hydraulic diameter is given by Equation (4). By that definition, the hydraulic diameter of a round cross-section channel is equal to its geometric diameter.

$$d_h = 4 \cdot A_{ch}/O_{ch} \qquad (4)$$

where:

A_{ch} - channel open area

O_{ch} - channel wetted perimeter.

For cellular catalyst substrates, the above definition of hydraulic diameter can also be conveniently expressed by the ratio of the open frontal area to the specific geometric surface area:

$$d_h = 4 \cdot (A_F/A) / a_g \qquad (5)$$

Equation (5) is valid for all cellular products with straight channels and can be used for all cell

configurations including sinusoidal channels of metallic substrates.

The GSA, OFA, and the channel hydraulic diameter are different for uncoated and coated substrates. The catalyst coating changes the apparent substrate wall thickness as well as, due to the washcoat fillets in the corners, the shape of the cell. Geometrical data which is available from substrate manufacturers usually refers to uncoated substrates. For best accuracy, parameters of coated substrates should be estimated and used when modeling the catalyst performance.

Bulk density of a catalyst substrate, ρ_b, is expressed by Equation (6).

$$\rho_b = \rho_m \cdot (1 - P) \cdot (1 - A_F/A) \quad (6)$$

where:

ρ_m - material density, kg/m^3

P - material porosity, dimensionless.

Total surface area, A_T, is a product of the catalyst volume, V, and its specific geometric surface area.

$$A_T = V \cdot a_g \quad (7)$$

Heat capacity of the catalyst substrate, C, may be calculated from Equation (8):

$$C = c_p \cdot \rho_b \cdot V \quad (8)$$

where:

c_p - specific heat capacity of the substrate material.

3. Substrate Configuration and Performance

The substrate configuration and geometry has to be carefully selected for a given catalyst application. The monolith matrix has an effect on all aspects of the catalyst performance, including:

- catalyst conversion efficiency
- catalyst light-off
- pressure drop
- resistance to fouling.

Emission control catalysts operate in the mass transfer controlled regime at high exhaust temperatures. Therefore, at a constant volume of the substrate, any changes which enhance the mass transfer conditions or increase the mass transfer surface area will increase the catalyst conversion efficiency. In particular, increasing the cell density improves the catalyst performance. The practical limit on cell density is set by the substrate manufacturing technologies, the catalyst coating technologies, as well as by the catalyst pressure drop which increases with smaller cells.

Catalyst substrate optimization for light-off performance has been conducted for gasoline engine applications. Even though diesels have lower cold start emissions than gasoline engines, light-off performance may be important in some applications, such as diesel cars in Europe. The influence of the substrate configuration on catalyst light-off is related to the warm-up time of the substrate walls. During light-off, catalysts work in the reaction kinetics controlled regime. The rate of reaction on a given catalyst depends on the catalyst temperature. The catalyst is deposited on the substrate walls which, at the moment of engine start-up, are cold. A certain time is required before the hot exhaust gases warm-up the substrate walls to the temperature which is required for catalytic reaction. Any changes to the substrate configuration which increase the heat transfer conditions or the heat transfer

surface area will also shorten the catalyst warm-up time and improve the cold start performance. It was suggested that the influence of catalyst washcoat, which increases the heat capacity of the substrate, is particularly important for cold start performance [Day 1997]. The washcoat can increase the catalyst heating time by as much as 40% compared to an uncoated support.

At a constant catalyst substrate volume, the exhaust gas pressure drop depends on the cell density, open frontal area, and the substrate cross-section (or aspect ratio). The pressure drop increases with increasing cell density and with decreasing open frontal area. Therefore, substrates with thin walls, which yield high open frontal areas, are desirable to minimize catalyst pressure drop. The pressure drop can be also minimized by shortening the catalyst and increasing its cross sectional surface area. This approach, however, is limited by its adverse effects on flow distribution, space constraints, and problems with canning of the monolith.

Fouling of the monolith channels by soot is another source of increased pressure drop in the diesel catalyst. Heavy-duty applications of high exhaust gas temperature are less likely to develop fouling problems. The particulates generated at high temperatures are "dry" and do not adhere to the substrate walls. At low temperatures, however, "wet" soot buildup may develop in the channels, which increases the pressure drop and decreases conversion efficiency. The risk of fouling increases at higher cell densities. Substrates of 300 cpsi and 400 cpsi have been successfully used on new, clean diesel engines. Lower cell density substrates of 200 cpsi or 300 cpsi are usually used for retrofit diesel applications to minimize the risk of plugging the substrate channels by soot.

4. Catalyst Pressure Drop

The total pressure drop across a catalyst substrate is a sum of three components: (1) pressure drop in the channels, ΔP_{ch}, (2) pressure loss at the channel entrance, ΔP_{in}, and (3) pressure loss at the channel exit, ΔP_{out}, represented by Equation (9).

$$\Delta P = \Delta P_{ch} + \Delta P_{in} + \Delta P_{out} \qquad (9)$$

The channel inlet and exit losses are associated with the contraction and expansion of gas at the inlet and outlet catalyst face, respectively. They are different from pressure losses in the inlet and outlet headers of the catalytic converter, which depend on the exhaust pipe diameter and the header geometry. The pressure drop in headers is not discussed here. The channel pressure drop is the most significant component in the total catalyst substrate pressure drop. The inlet and outlet pressure drop constitutes in most cases less than 10% of the total pressure drop. The channel portion of substrate pressure drop is directly proportional to the gas flow rate. The inlet and outlet pressure drop contributions increase with the square of flow rate.

The frictional pressure drop of exhaust gases in substrate channels can be calculated using the Darcy equation:

$$\Delta P_{ch} = 4f \cdot (L/d_{ch}) \cdot (\rho v^2/2) \qquad (10)$$

where:

f - Fanning friction factor, dimensionless,

L - substrate length, m,

d_{ch} - channel diameter, m,

ρ - gas density, kg/m^3,

v - linear velocity of gas in channels, m/s,

ΔP - pressure drop, Pa.

The hydraulic diameter, d_h, is used instead of d_{ch} for non circular channel cross-sections.

The gas velocity, v, can be calculated as follows:

$$v = W / (\rho \cdot A_F) \quad (11)$$

where:

W - total mass flow rate, kg/s,

A_F - substrate open frontal area, m^2.

The dimensionless Reynolds number N_{Re} is used in fluid mechanics as a criterion for the flow regime. Laminar flow is observed at $N_{Re}<2100$ for the flow of fluids in pipes and channels. In all practical cases, monolithic catalyst substrates operate in the laminar flow regime. The Reynolds number is defined by the following equation:

$$N_{Re} = v \cdot d_{ch} \cdot \rho / \mu \quad (12)$$

where:

μ - dynamic gas viscosity, kg/(m·s).

The laminar flow Fanning friction factor can be calculated as follows:

$$f = K / N_{Re} \quad (13)$$

where the magnitude of K depends on channel cross-section, Table 1.

Table 1
Fanning Friction Factor

Channel Cross Section	$K = (f \cdot N_{Re})$
Round	16.00
Square	14.23
Equilateral Triangle	13.33
Sinusoidal*	10.96
* - duct open height to open width ratio 0.425	

The above friction factors were compiled from the literature [Perry 1984][Rohsenow 1993]. Laboratory evaluation of ceramic monoliths with square cells and metal monoliths with sinusoidal cells showed very good correlation with the respective coefficients in Table 1 [Day 1997a].

Since the substrate inlet and outlet pressure losses are relatively insignificant in the total catalyst pressure drop, there has been little experimental data published which would relate specifically to catalyst substrates. The inlet and outlet pressure losses are likely to be influenced by the test equipment, thus, making the experimental studies more difficult. The exhaust gas flow which is always laminar inside channels can be turbulent or transitional outside the catalyst substrate.

It is convenient to express the inlet and outlet pressure drop by a formula with structure similar to that of Equation (10):

$$\Delta P_{in/out} = K_{in/out} \cdot (\rho v^2/2) \quad (14)$$

The friction coefficients K_{in} and K_{out} can be estimated using known methods for pressure losses due to gas contraction and expansion. For contraction K_{in} can be calculated from the substrate open frontal area as follows:

$$K_{in} = -0.415 \cdot A_F/A + 1.08 \quad (15)$$

Equation (15) has been computed from literature data for laminar flow [VDI 1992]. It is believed that in some situations the calculated pressure drop may be overestimated. Coefficients K_{in} for turbulent flow are approximately 50% lower than those from Equation (15). Frictional losses for transitional Reynolds numbers range between those for the laminar and turbulent losses.

The friction coefficient for gas expansion with turbulent flow can be calculated from the simple Borda-Carnot equation:

$$K_{out} = (1 - A_F/A)^2 \qquad (16)$$

By combining Equation (9) with the Darcy Equation (10) and Equation (14), the total catalyst substrate pressure drop can be expressed as follows:

$$\Delta P = [4f \cdot (L/d_{ch}) + K_{in} + K_{out}] \cdot (\rho v^2/2) \qquad (17)$$

References

Day, J.P., 1997. "Substrate Design for Cold Start", SAE Advancements in Automotive Catalyst Technology TOPTEC, Dearborn, MI

Day, J.P., 1997a. "Substrate Effects on Light-Off - Part II: Cell Shape Contributions", SAE 971024

Jatkar, A.D., 1997. "A New Catalyst Support Structure for Automotive Catalytic Converters", SAE 971032

Kikuchi S., et al., 1999. "High Cell Density and Thin Wall Substrate for Higher Conversion Ratio Catalyst", SAE 1999-01-0268

Marsh, P., et al., 2001. "Application Guideline to Define a Catalyst Layout for Maximum Catalytic Efficiency", SAE 2001-01-0929, http://www.emitec.com/pdf/SAE2001-01-0929.pdf

Perry, R.H., 1984. "Perry's Chemical Engineers' Handbook", McGraw-Hill, 6th edition

Rohsenow, W.M., et al. (editors), 1993. "Handbook of Heat Transfer Fundamentals", McGraw Hill, New York, 2nd edition

Stankiewicz, E.P., et al., 1998. "Properties and Performance of UltraCat Open-Cell Silicon Carbide Foam Catalyst Substrate", SAE 980669

VDI, 1992. "VDI-Waermeatlas, 6. Aufl.", VDI-Verlag Duesseldorf

###